



BioStudio -T

Cell Observation Device

Nikon's BioStudio-T was designed specifically for research applications in the field of regenerative medicine and stem cell biology and for use in cell manufacturing facilities. A compact live-cell imaging microscope, the BioStudio-T fits inside most incubators and is compatible with a variety of sterilization methods including vaporized H₂O₂. The fixed-stage, scanning lens system also provides a superior solution for long-term time lapse imaging and large image acquisition.

For more information on the BioStudio-T,
visit www.microscope.healthcare.nikon.com/biostudio-t

Role of Activator Protein-1 Complex on the Phenotype of Human Osteosarcomas Generated from Mesenchymal Stem Cells

STEFANO GAMBERA ^{a,†} ANDER ABARRATEGI ^{a,b,†} MIGUEL A. RODRÍGUEZ-MILLA,^a FRANCISCA MULERO,^c SOFÍA T. MENÉNDEZ,^{d,e} RENÉ RODRIGUEZ ^{d,e} SAMUEL NAVARRO,^{e,f} JAVIER GARCÍA-CASTRO ^a

^aCellular Biotechnology Unit, Instituto de Salud Carlos III, Madrid, Spain; ^bHaematopoietic Stem Cell Laboratory, The Francis Crick Institute, London, UK; ^cMolecular Image Core Unit, Spanish National Cancer Research Centre, Madrid, Spain; ^dHospital Universitario Central de Asturias—Instituto de Investigación Sanitaria del Principado de Asturias and, Instituto Universitario de Oncología del Principado de Asturias, Oviedo, Spain; ^eCIBER de Cáncer (CIBERONC), Madrid, Spain; ^fPathology Department, University of Valencia, Valencia, Spain

Correspondence: Javier García-Castro, Ph.D., Unidad de Biotecnología Celular, Instituto de Salud Carlos III, Lab. 51-00-036, Ctra Majadahonda-Pozuelo, Km 2, E-28220, Majadahonda, Madrid, Spain. Telephone: 34-918-223-288; e-mail: jgcastro@isciii.es

†Contributed equally.

Received January 11, 2018; accepted for publication May 28, 2018.; first published online in *STEM CELLS EXPRESS* July 12, 2018.

<http://dx.doi.org/10.1002/stem.2869>

This is an open access article under the terms of the Creative Commons Attribution-NonCommercial License, which permits use, distribution and reproduction in any medium, provided the original work is properly cited and is not used for commercial purposes.

Key Words. Mesenchymal stem cells • Osteosarcoma • p53 • Rbc-JUN • c-FOS

ABSTRACT

Osteosarcoma (OS) is a highly aggressive bone tumor that usually arises intramedullary at the extremities of long bones. Due to the fact that the peak of incidence is in the growth spurt of adolescence, the specific anatomical location, and the heterogeneity of cells, it is believed that osteosarcomagenesis is a process associated with bone development. Different studies in murine models showed that the tumor-initiating cell in OS could be an uncommitted mesenchymal stem cell (MSC) developing in a specific bone microenvironment. However, only a few studies have reported transgene-induced human MSCs transformation and mostly obtained undifferentiated sarcomas. In our study, we demonstrate that activator protein 1 family members induce osteosarcomagenesis in immortalized hMSC. c-JUN or c-JUN/c-FOS overexpression act as tumorigenic factors generating OS with fibroblastic or pleomorphic osteoblastic phenotypes, respectively. *STEM CELLS* 2018;36:1487–1500

SIGNIFICANCE STATEMENT

During the last decades survival rate for patients with nonmetastatic osteosarcoma (OS) has increased notably, but metastatic and refractory OS maintain a low survival rate. The development of more effective OS treatments requires a deep knowledge about the origin and development of this tumor.

INTRODUCTION

Osteosarcoma (OS) is a highly malignant tumor represented in children and young adults, which is the most frequent primary bone tumors of non-hematopoietic origin [1]. OS mostly arises intramedullary in the epiphysis of the growing bone like femur, tibia, and humerus [2]. Histologically, OS is a malignant mesenchymal tumor formed by spindle-shaped cells producing aberrant immature bone matrix, also called osteoid [3]. OS is a heterogeneous tumor and its classic conventional form can be further subdivided into osteoblastic, chondroblastic, or fibroblastic, among other subtypes, depending on the main matrix produced by the tumor [3]. With multi-agent chemotherapy and surgical resection, the 5-year survival rate for OS patients is still 65%–70% [2].

OS pathogenesis is a complex process which is not completely understood. Patients with hereditary syndromes like retinoblastoma (RB) and Li-Fraumeni are predisposed to OS development; RB1 and TP53 are also frequently mutated in

sporadic cases of OS [4]. Those genes regulate processes like DNA replication, cell cycle arrest, apoptosis, senescence, and DNA damage response. There is increasing evidence that OS most likely derives from mesenchymal stem cell (MSC) or MSC-derived cell types, although the exact cell of origin is unclear [2]. Murine models show that it is possible to induce OS formation if deleting some of the previously mentioned genes along the osteogenic differentiation lineage [5, 6] or if cells are implanted in the proper osteoinductive microenvironment [7]. Furthermore, mouse MSCs were also used to generate other sarcomas models by the introduction of FUS/DDIT3, EWSR1/FLI1, PAX/FOXO1, and SYT-SSX-1 fusion genes generating myxoid liposarcoma, Ewing's sarcoma, rhabdomyosarcoma, and synovial sarcoma [8]. These studies underlined the importance of the microenvironment and the type of genetic hits in sarcoma phenotype originated by mouse MSCs transformation.

In contrast, human MSCs (hMSC) transformation is a more complex process. Human

spindle cell sarcomas [9, 10], tumors with smooth muscle and bone-forming cells [11], and undifferentiated sarcomas [12] were induced introducing hTERT overexpression, p53 and RB pathways inhibition, and oncogenic RAS mutations in hMSC. One study demonstrated that hMSC transformation can be induced by RB knockdown and c-MYC overexpression, generating bone-like tumors [13]. In addition, enforced expression of fusion oncogenes in wild-type hMSCs was not sufficient to induce sarcomagenesis [8, 14]. However, the expression of FUS/DDIT3 was able to re-direct the sarcomagenic program of previously transformed hMSCs and induced the formation of myxoid liposarcomas in vivo [15]. Interestingly, in all the studies, several genetic hits were required to transform hMSCs and confirmed the idea that specific mutations can force tumor phenotype.

The activator protein 1 (AP-1) complex is a transcriptional regulator that can be formed by Jun, Fos, and members of the activating transcription factor (ATF) family which binds as homo- and/or heterodimers and regulates promoter regions of various genes [16]. AP-1 complex regulates proliferation, differentiation, and bone metabolism. Various members of the AP-1 complex are expressed differentially during osteoblast differentiation [17], where c-Fos knockout alters endochondral differentiation [18] and c-Jun is essential for embryonic development [17]. Both c-Fos and c-Jun upregulations are seen in high-grade OS suggesting their involvement in osteosarcomagenesis [19]. Similarly to AP-1, nuclear factor- κ B (NF- κ B) is a dimeric transcription factor complex implicated in the regulation of cell proliferation, survival, neoplastic transformation, and immune and inflammatory response. Despite AP-1 and NF- κ B binds to distinct enhancer motif, it was described synergism and cross-coupling between the different members of these transcription factors families in cancer [20, 21].

In this article, we demonstrate that the overexpression of c-JUN and c-JUN/c-FOS in immortalized hMSC is sufficient to induce cell transformation and OS formation. Moreover, depending on the AP-1 members overexpressed, tumors develop different OS phenotypes. Thus, c-JUN overexpression generates fibroblastic OS and the double expression of c-JUN/c-FOS induces pleomorphic osteoblastic phenotype.

MATERIALS AND METHODS

Cell Culture

Immortalized hMSCs defined as 3 HITs or just 3H cells in the text were kindly provided by Dr. Funes. Those cells are hMSC overexpressing hTERT and HPV-16 E6/E7, which extend cell lifespan in culture and abrogate p53 and pRB function, respectively [9], although they are not tumorigenic when inoculated in immunodeficient mice. Normal hMSCs were isolated from healthy donors after signing an informed consent. All cell lines were cultured in Dulbecco's modified Eagle's medium (DMEM) supplemented with 10% fetal bovine serum, 1% penicillin/streptomycin, and 2 mM L-glutamine (Lonza, Basel, Switzerland) and routinely tested for mycoplasma infection.

c-DNAs of c-FOS and c-JUN were cloned into pOTB7 and pWPI plasmids to generate lentiviral vectors able to induce the constitutive expression of c-FOS and c-JUN; each vector carries TdTomato and enhanced green fluorescent protein (EGFP) as reporter fluorescent markers, respectively. Two additional pOTB7

and pWPI plasmids carrying only TdTomato or EGFP fluorescent markers were used to generate empty control vectors. Lentiviral particles were produced in HEK-293 cells by transient calcium phosphate transfection. Supernatants were collected 48 hours after transfection, ultracentrifugated, and the concentrated lentiviral particles were stored at -80°C . Then, cells were transduced with these lentiviral vectors generating 3 HIT cells overexpressing c-JUN (3H-JUN) or c-JUN and c-FOS (3H-JUN/FOS) genes; 3 HITs cells were also transduced with empty vectors to generate a control cell line (3H- \emptyset). Four days after transduction, cells were fluorescence-activated cell sorted and shortly amplified in vitro to generate a cell stock which was used in the following experiments.

In Vitro Growth Assays

For proliferation assay, 2×10^5 cells were seeded in 75 cm² flasks. Cells were trypsinized, counted, and replated in the same conditions every day during 48 hours. Alternatively, 2.5×10^3 cells were seeded onto each well of E-Plate L8 plates within an iCELLigence system (ACEA Biosciences, San Diego, CA) and left to proliferate in growth media at 37°C with 5% CO₂ for 10 days. In the iCELLigence system, cells adhere to micro-electrodes which continuously measure alterations in electrical impedance, thus allowing the real-time monitoring of cell proliferation. Cell status is expressed as normalized cell index (Cell index relative to that of the time the cells need to attach to the plates, 9 hours). Data were analyzed in the real-time cell analysis (RTCA) data analysis software 1.0 (ACEA Biosciences). In cell cycle experiments, 60% confluence cells were fixed using 70% ice-cold ethanol, permeabilized with a solution of phosphate-buffered saline (PBS) with Triton 0.1%, and stained with 4',6-diamidino-2-phenylindole (DAPI) (10 $\mu\text{g}/\text{mL}$) (ThermoFisher, Waltham, MA) for DNA labeling. All cells were analyzed in a BD LSRFortessa flow cytometer (BD Bioscience, Madrid, Spain). Cell cycle statistics were obtained with FlowJo7.6 (FlowJo, Ashland, OR). For multilayer growth study, cells were seeded subconfluent and allowed to reach complete confluency. Cells were stained using Texas Red-X phalloidin and DAPI according to manufacturer protocol (ThermoFisher). A confocal multispectral microscope Leica TCS-SP5 (Leica Microsystems, Wetzlar, Germany) was used in this experiment. Stacks of 20 layers were acquired and orthogonal sections were processed using Leica LAS AF (Leica Microsystems). Colony formation in agar was assessed with the Cytoselect 96-well cell transformation assay kit (Cell Biolabs, San Diego, CA), following manufacturer's instructions. Briefly, 2×10^3 cells were suspended in soft agar and plated in each well; each experiment was performed by duplicate and repeated three times. Colony formation was screened by optical microscopy twice a week for 21 days. Wound healing assays were performed with confluent cells and a pipette tip was used to make a wound in cell monolayer. Images were obtained at different time points during 24 hours. For cell senescence studies, cells were fixed and incubated overnight with X-gal solution (pH 6.0) as described previously [22]. Each experiment was performed by duplicate and repeated three times.

Drug Sensitivity Assay

In vitro drug sensitivity assay was performed by seeding 5×10^3 cells per well in 96-well plates ($n = 6$) and incubating cells in different cisplatin concentrations (Ebewe pharma 10 mg/20 ml). After 24 hours, cells were washed with PBS and incubated with 3-[4,5-dimethylthiazol-2-yl]-2,5-diphenyltetrazolium bromide (MTT) solution in DMEM without phenol red (0.5 mg/mL).

After 3-hour incubation in darkness, cells were washed again with PBS and 100 μ l of dimethyl sulfoxide was added to each well. MTT absorbance was acquired at 570 nm. Data were normalized subtracting a background value, as ratio of absorbance test (test)/absorbance control (no treatment).

Cytokines Profiling

Approximately 1×10^5 cells were seeded in a p6 well with complete DMEM; after attachment, cells were washed with PBS and incubated with serum-free DMEM. Supernatants were collected 24 hours later and pro-inflammatory cytokine pattern was analyzed using Proteome Profiler Human Cytokine XL Array kit according to the manufacturer's indications (R&D Systems, Minneapolis, MN). Secreted cytokine profile was measured semi-quantitatively by pixel density of duplicated spots with ImageJ. Data were normalized subtracting background.

NF- κ B Activity Assay

The activation of NF- κ B was evaluated using a luciferase reporter system [23]. 1.5×10^5 cells were seeded in a p6 well with complete DMEM; after attachment, cells were transduced overnight with a non-replicative lentiviral vector that contains the pHAGE NF- κ B-TA-LUC-UBC-GFP-W plasmid (Addgene plasmid #49343). Then, cells were amplified for three passages and finally plated in P96 wells. After 24 hours, cell lysis for total protein extraction was carried out and luciferase activity was assayed with the Luciferase Assay System (Promega Corporation, Madison, WI). Luminescent signal was normalized against transduction efficiency, which was estimated by green fluorescent protein expression.

Adipogenic, Osteogenic, and Chondrogenic Cell Differentiation

Cells were differentiated using adipogenic, osteogenic, or chondrogenic MPCs differentiation BulletKit (Lonza, Besel-Switzerland), following manufacturer's instructions. For the assessment of adipogenic differentiation, cells were fixed in 4% paraformaldehyde and stained with oil red O (Sigma-Aldrich, St. Louis, MO), osteogenic differentiation was evaluated by Alizarin red staining (VWR, Radnor, PA), and chondrogenic differentiation was determined by Alcian blue dye (Sigma, Kawasaki, Japan) on micromass pellets previously included in cryo-embedding media (Sakura Finetek, Alphen aan den Rijn, Netherlands).

Western Blot Analysis

Proteins were extracted from subconfluent cultures by incubation on ice with lysis buffer (1% NP-40, 50 mM Tris pH 7.5, 10 mM tetrasodium pyrophosphate, 150 mM NaCl, 10 mM NaF, 1 mM PMSF, 20 mM β -glycerophosphate, 0.1 mM sodium orthovanadate, and 1:100 protease inhibitor cocktail from Sigma, St. Louis, MO). DC Protein Assay system (Bio-Rad, Hercules, CA) was used for protein quantification. Approximately 50 μ g of proteins per lane were loaded in 10% SDS-polyacrylamide gel electrophoresis gels and, after electrophoretic separation, blotted onto poly(vinylidene fluoride) membranes (Bio-Rad, Hercules, CA). Blots were incubated with primary and secondary antibodies (Supporting Information Table S1) and detected using Immobilon Western Chemiluminescent HRP Substrate (Millipore, Burlington, MA).

Global Transcriptional Analysis and Study

Ten days after transfection, total RNA was extracted from transduced cells. RNA (250 ng) from each biological sample was processed and the transcriptional profile was analyzed with the use of the GeneChip Affymetrix platform and the GeneChip Human Gene 2.0 ST Array (Santa Clara, CA). Specific protocols, details, and expression data are available in the Gene Expression Omnibus functional genomics data repository (<http://www.ncbi.nlm.nih.gov/geo/>) under the accession number GSE79158. Data were analyzed using Bioconductor 2.12 (<http://www.bioconductor.org>) running on R 3.0.0. Probeset expression measures were calculated with the Affymetrix package's Robust Multichip Average default method. Differentially expressed genes were assessed between samples using an empirical Bayes *t*-test (limma package) and *p* values were adjusted for multiple testing by the Benjamini-Hochberg method [24]. Any probe sets that exhibited an adjusted *p* value of .05 were called differentially expressed. All genes on the Affymetrix chip were used as the background for enrichment analyses. The *p* value was corrected using the Benjamini and Hochberg multiple testing correction method. Differentially expressed genes were screened for AP-1 binding site using transcription factor binding sites predictor UCSC-TFBS function in DAVID. Differentially expressed genes were used to look for enrichment using Enricher tool (<http://amp.pharm.mssm.edu/Enrichr/>) in Gene Ontologies (GO Molecular Functions, 2017) and pathways (KEGG, 2016); Fisher exact test was used to generate and compute ranking and SD from expected rank for each term in the gene-set library and finally calculating a z-score to assess the deviation from the expected rank. Adjusted *p* < .05 was considered significant. For GO (GO-Biological process, 2017), only GO terms with enrichment Z-score of ≤ -1.40 were considered significant. Combined score is computed by taking the log of the *p* value from Fisher exact test and multiplying that by the z-score of the derivation from the expected rank were judged to be statistically significant. Alternatively, enrichment of pathways and biological GO terms were assessed using Gene Set Enrichment Analysis (GSEA, v2.0). Gene-sets were downloaded from MSigdb (<http://software.broadinstitute.org/gsea/msigdb>) for GSEA. Gene sets statics are indicated in each figure.

OS Meta-analysis of Clinical Samples

Microarray-based search of c-JUN, c-FOS, dipeptidyl peptidase IV (DPPIV), platelet-derived growth factor (PDGF)-A, NFKB1, NFKB2, and RELB mRNA expression levels in clinical samples, its correlation to overall survival, and tumor phenotype, were conducted using the Mixed OS—Kuijjer dataset [25], which is available from the online R2: genome analysis and visualization platform (<http://r2.amc.nl>). The Kuijjer database contains microarray data of a cohort of 84 pretreatment diagnostic biopsies of high-grade OSS; those data are associated with patient's survival and tumor phenotype. Two smaller cohorts of fibroblastic (*n* = 9) and osteoblastic (*n* = 55) OS were used for sub-specific gene expression comparisons according to tumor phenotype.

Animal Procedures

Immunodeficient non-obese diabetic/severe combined immunodeficient mice of 10–12 week-old were used in the

experiments. Cells were inoculated either subcutaneously (10^6 cells per mouse) or through intra-bone marrow (5×10^5 cells per mouse). Cells were resuspended in PBS and filtered through a 70- μm nylon filter for inoculation. For intra-bone marrow administration, anesthesia was induced by intraperitoneal injection of a mixture of xylazine (Rompun, Bayer, Leverkusen, DE)–ketamine (Imalgene 1,000, Merial, Lion, FR). The right hind limb was bent 90° to allow drilling tibial plateau with a 25G needle before cell inoculation with a 27G needle. Ectopic bone-like implants were realized embedding cells in biphasic calcium phosphate crystals (Biomatlante, Vigneux-de-Bretagne, France). In some experiments, bone morphogenic protein 2 (BMP2) (Noricum, Madrid, Spain) was also included as osteogenic promoting factor. For a detailed protocol of ectopic bone-like implants follow the previously described protocol [7, 26]. Procedures were performed with the approval of the institutions Animal Care and Use Committee, following EU Directive for animal experiments and in a specific pathogen-free environment.

Histological Processing

Samples were washed twice with cold PBS and fixed 24 hours in 10% neutral-buffered formalin. Tumors were decalcified with 4% hydrogen chloride/4% formic acid in water during 3 days or alternatively with 17% EDTA (Osteosoft, Millipore, Burlington, MA) during 7 days. Then samples were processed for sectioning, paraffin embedded, and sectioned (8 μm) for histological studies. Hematoxylin/eosin, Masson's trichrome, and Alcian blue stainings were performed.

Micro-computed Tomography

Formalin-fixed samples were imaged in an eXplore Vista μCT system (GE Healthcare, Chicago, IL), with an X-ray tube voltage of 50 kV and a current of 200 μA . The scanning angular rotation was 180° , the angular increment was 0.40° , and the voxel resolution was 50 μm . Data sets were reconstructed and segmented into binary images (8-bit BMP images) for the subsequent image processing and 3D surface reconstructions using MicroView ABA 2.2 software (GE Healthcare).

Immunostaining

Immunohistochemistry (IHC) studies were performed by standard methods; heat antigen retrieval was performed when required in IHC studies (see primary unconjugated antibodies used in Supporting Information Table S1). Secondary fluorescent antibodies were from Invitrogen and secondary biotinylated antibodies were from Jackson (Bar Harbor, ME). Texas Red-X phalloidin (Invitrogen, Carlsbad, CA) was used for actin staining.

Statistics

Experiments were performed at least by triplicate. Data were expressed as means \pm SD or SEM. Student *t* test and analysis of variance (ANOVA) analysis were performed using Graph Pad Prism 6 software (La Jolla, CA). One-way ANOVA was used to compare statistical difference in more than two groups, with Bonferroni post hoc test. For multiple comparisons, a confidence interval of 95% was adopted and only *p* values inferior to .05 were considered statistically significant. *p* value is indicated in each panel and figure (*, $p \leq 0.05$; **, $p \leq 0.01$; ***, $p \leq 0.001$; ****, $p \leq 0.0001$).

RESULTS

AP-1 Overexpression Induces Transformation of Immortalized hMSC

First, we use lentiviral gene transfer to overexpress c-JUN or c-JUN/c-FOS in wild-type hMSC. We observed no changes in the proliferation rate, cell cycle distribution, or senescence levels after the overexpression of these factors (Supporting Information Fig. S1). In addition, no tumor growth was detected when these cells were inoculated into immunodeficient mice. Since it was reported that several oncogenic events are needed to fully transform hMSCs [8, 9], we next use the same vectors in hMSC previously immortalized through the sequential introduction of several oncogenic hits (i.e., ectopic expression of hTERT and inactivation of p53 and Rb by the expression of the E6 and E7 antigens of HPV-16; MSC-3H cells). The efficient generation of cells overexpressing c-JUN (3H-JUN) or c-JUN and c-FOS (3H-JUN/FOS) was confirmed both by Western blotting (Fig. 1A) and flow cytometry analysis of the fluorescence produced by the reporter genes included in c-JUN and c-FOS lentiviral vectors (Fig. 1B). Interestingly, flow cytometry study also reveals relevant changes in cellular morphology, being cell size and complexity reduced after c-JUN and specially c-JUN and c-FOS expression (Fig. 1C); those changes in cell morphology were also confirmed by light microscopy (Fig. 1D). *in vitro* proliferation assays showed that 3H-JUN cells proliferate faster than control and 3H-JUN/FOS cells (Fig. 1E). In addition, both 3H-JUN and 3H-JUN/FOS showed a reduction in the G_1 phase and a concomitant increase in S and G_2/M of the cell cycle as compared to control cells (Fig. 1F). Moreover, immortalized hMSC overexpressing c-FOS and/or c-JUN showed evident signs of cell transformation *in vitro*. Thus, 3H-JUN/FOS lost contact inhibition and started to grow forming multi-layered clumps (Fig. 1G). In addition, both 3H-JUN and 3H-JUN/FOS cells were able to grow forming colonies in soft agar (Fig. 1H). Furthermore, wound healing assays showed that the expression of c-JUN or c-JUN/c-FOS did not affect the migration ability of immortalized hMSCs (Fig. 1I), and finally, 3H-JUN and 3H-JUN/FOS cells displayed a highly increased sensitivity to chemotherapeutic drugs like cisplatin (Fig. 1L). In summary, these data (Fig. 1) support that AP-1 overexpression contributed to the transformation of immortalized hMSCs *in vitro* inducing consistent changes in their growth properties and sensitizing them to cytotoxic drugs.

c-JUN and c-JUN/c-FOS Overexpression Unbalance Similar Cellular Pathways

Next, we performed gene expression analysis to identify molecular pathways altered by the overexpression of c-JUN and c-JUN/c-FOS in immortalized hMSCs (Fig. 2). We found that 587 and 779 genes were differentially expressed in 3H-JUN and 3H-JUN/FOS, respectively, relative to control 3H cells (Fig. 2A). In total, 53.3% of these altered genes were commonly altered in both cell lines, while 12.6% and 34.1% of the genes were specifically dysregulated in 3H-JUN and 3H-JUN/FOS cells. A predictive transcription factor binding study identified those altered genes presenting AP-1 promoter responsive elements in their sequence (Supporting Information Table S2). Among this subset of genes, 86 were exclusively overexpressed in 3H-JUN/FOS cells, 25 genes were exclusively overexpressed in 3H-JUN cells,

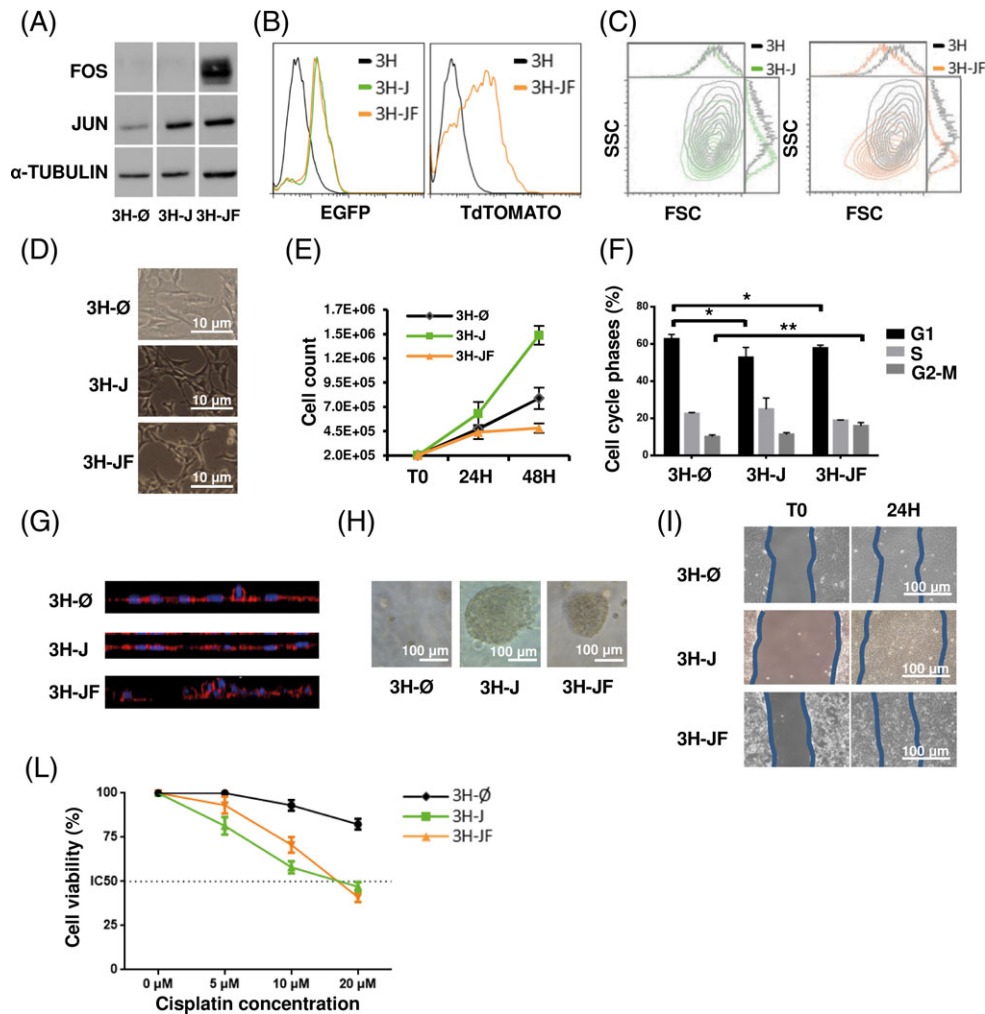


Figure 1. Expression of c-JUN or c-JUN/c-FOS induces cell transformation in vitro. **(A):** c-JUN and c-FOS protein levels in control 3H (3H-Ø), 3H-JUN (3H-J), and 3H-JUN/FOS (3H-JF) cells analyzed by Western blot. α -Tubulin levels were used as loading control. Uninformative lanes were cut out. **(B):** Flow cytometry evaluation of EGFP (left panel) and TdTomato (right panel) reporter gene expression levels in control 3H (black line), 3H-JUN (green line), and 3H-JUN/FOS (orange line) cells. **(C):** Size (FSC) and complexity (SSC) changes detected in contour plots comparing 3H-Ø cells (black contour) with 3H-J (green; left panel) or 3H-JF (orange; right panel). **(D):** Representative light microscopy images of 3H-Ø, 3H-J, and 3H-JF cell lines showing changes in cellular morphology. **(E):** in vitro proliferation of 3H-Ø, 3H-J, and 3H-JF cell lines. **(F):** Flow cytometry quantification of the percentage of cells in each phase of the cell cycle; cell lines are indicated on the x-axis. **(G, H):** Representative images of in vitro transformation assays showing the ability of 3H-JF cells to grow forming multilayered clumps (G), and the ability of 3H-J and 3H-JF cells to form colonies in soft-agar (H). **(I):** Representative images of the wound healing assay indicating no differences in cell mobility between 3H-Ø, 3H-J, and 3H-JF cell lines. **(J):** Cell viability (MTT assay) measured after treating 3H-Ø, 3H-JUN, and 3H-JUN/FOS cells for 24 hours with the indicated concentrations of cisplatin. Abbreviations: EGFP, enhanced green fluorescent protein; FSC, forward scatter; SSC, side scatter.

Table 1. In vivo tumorigenesis

	T.I.	Incidence	Latency	VIM	KI-67	OSN	OSC	S-100	COLL2	Diagnosis
hMSC-cJUN	s.c.	0/6	-							Not tumorigenic
hMSC-cFOS	s.c.	0/6	-							Not tumorigenic
3H-Ø	s.c.	0/15	-							Not tumorigenic
	Tibia	0/8	-							
3H-JUN	s.c.	13/13	60–150	+	50%	+	+	-	-	Fibroblastic OS
	Tibia	2/4	150–170	+	5%	+	+	-	-/+	Fibroblastic/low grade OS
3H-JUN/FOS	s.c.	14/14	20–60	+	80%	+	-/+	-	-/+	Pleomorphic/osteoblastic OS
	Tibia	5/5	32–40	+	20%	+	+	-/+	-	Pleomorphic/osteoblastic OS

Incidence indicates the number of animals developing tumors over the total of the inoculated animals. Latency was calculated as the time (expressed in days) needed to reach a tumor volume of 1 cm³.

Abbreviations: COLL2, collagen type II; hMSC, human mesenchymal stem cell; OS, osteosarcoma; OSC, osteocalcin; OSN, osteonectin; S100, S100 calcium binding protein; T.I.: tumor inoculation procedures divided in subcutaneous ectopic (s.c.) and orthotopic (Tibia) inoculation; VIM, human vimentin.

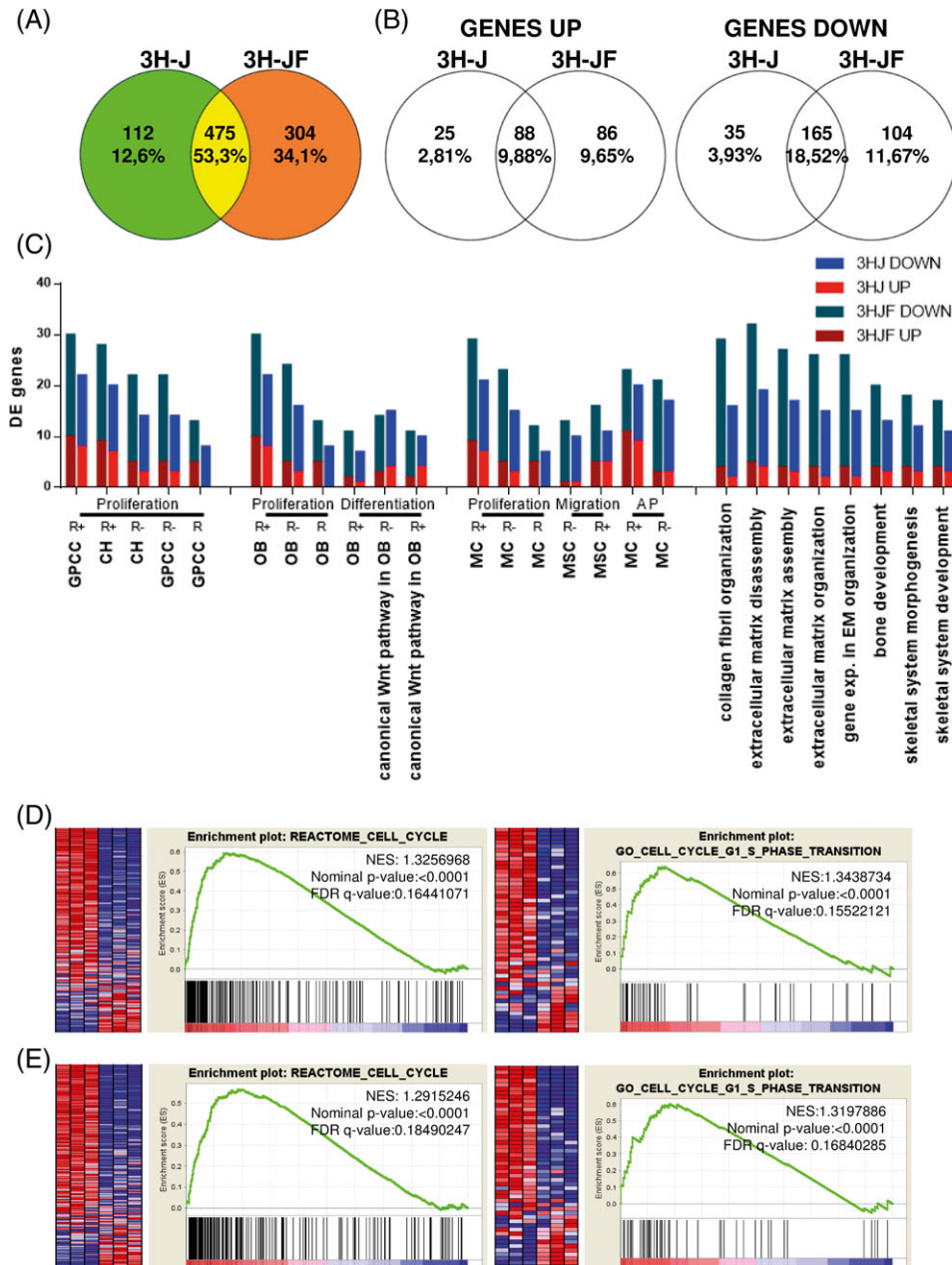


Figure 2. Gene expression analysis of 3H-JUN and 3H-JUN/FOS cells. **(A, B):** Venn diagrams representing the number, percentage, and overlay of genes differentially expressed in 3H-JUN (3H-J) and 3H-JUN/FOS (3H-JF) relative to control 3H-0 cells (A), or the same analysis restricted to those genes presenting a transcription factor binding site for AP1 and subdivided into upregulated (left panel) and downregulated (right panel) genes (B). **(C):** Gene Ontology terms enriched signatures in biological process of proliferation, differentiation, and apoptosis of chondrocytes, grow plate cartilage chondrocytes, osteoblasts, mesenchymal cells, and mesenchymal stem cells. Positive regulation (R+) and negative regulation (R-) signatures are presented; R indicates regulation signature not included into stimulating or inhibitory processes. Also changes in collagen and matrix organization, assembly and disassembly like bone and skeletal system development were enriched. **(D, E):** Cell cycle-related Gene Set Enrichment Analysis enriched plots in 3H-JUN (D) and 3H-JUN/FOS cells (E). Abbreviations: AP, apoptosis; CH, chondrocytes; GPCC, grow plate cartilage chondrocytes; MC, mesenchymal cells; MSC, mesenchymal stem cells; OB, osteoblasts.

and 88 genes were commonly overexpressed (Fig. 2B). Similarly, 104 and 35 genes were specifically downregulated in 3H-JUN/FOS and 3H-JUN, respectively, while 165 genes were commonly downregulated (Fig. 2B). KEGG pathways and GO Molecular Functions terms analysis of the commonly dysregulated genes identified the enrichment of differentially expressed genes in pathways related to cancer, including extracellular matrix receptor interactions, Wnt and PI3K/Akt signaling, cell adhesion

molecules, growth factors, cytokines, and chemokines (Supporting Information Table S2). Among the private differentially expressed genes in 3H-JUN/FOS, most of the altered genes were tyrosine and threonine kinases, with enrichment in MAPK signaling, osteoclast differentiation, and focal adhesion, as other additional alteration in cancer pathways and PI3K/Akt signaling (Supporting Information Table S2). The total amount of differentially expressed genes, even not presenting AP-1 transcription

factor binding site, matched the enrichment of different GO terms implicated in proliferation, differentiation, migration, and apoptosis of chondrocyte, osteoblast, and MSC (Fig. 2C). Furthermore, we also found enriched signatures related to bone and skeletal development as extracellular matrix organization (Fig. 2C) (The complete GO terms enrichment analysis is available separately in Supporting Information Tables S3, S4). Notably, the alterations of cell cycle-related pathways were further confirmed by GSEA (Fig. 2D, 2E).

c-JUN or c-JUN/c-FOS Overexpression Does Not Affect the *in vitro* Osteochondrogenic Differentiation Potential

To define whether the expression of AP-1 transcription factors could affect the differentiation potential of immortalized hMSCs, we tested the ability of 3H-JUN and 3H-JUN/FOS cells to undergo adipogenic, osteogenic, and chondrogenic differentiation *in vitro* (Fig. 3). 3H-JUN cells displayed an impaired pattern of adipogenic differentiation similar to that previously observed for 3H-Ø cells [15], whereas 3H-JUN/FOS cells were completely unable to form lipid droplets filled adipocytic-like cells when they were cultured in adipogenic medium. In contrast, all the cell lines efficiently generated alizarin red-positive calcium deposits under osteogenic stimulation and alcian blue-positive matrix deposits after micromass culture in chondrogenic assays.

In summary, our data indicate that c-JUN and c-JUN/c-FOS overexpression in immortalized hMSCs does not alter their osteochondrogenic potential *in vitro*.

Ectopic *in vivo* Implantation of 3H-JUN and 3H-JUN/FOS Cells Generates Phenotypically Different OSs

To assay the *in vivo* tumorigenic potential, we first inoculated immunodeficient mice subcutaneously with control cells or cells overexpressing AP-1 transcription factors. Opposite to control 3H-Ø cells, which were unable to initiate tumor growth, both 3H-JUN and 3H-JUN/FOS cells generated tumors with 100% of incidence, showing 3H-JUN/FOS cells a shorter latency (Table 1). Histological analysis of these tumors confirmed the development of two phenotypically different types of OSs. Hematoxylin/eosin and Masson's trichrome staining revealed that 3H-JUN (Fig. 4A) and 3H-JUN/FOS (Fig. 4B) tumors presented fibroblastic and pleomorphic osteoblastic phenotypes, respectively. In the first case, the characteristic osteoid matrix was organized in fibrillary structures, while in the second, osteoid matrix were surrounding cells presenting different morphologies, including areas of a myxoid chondrogenic phenotype (Fig. 4). Immunohistochemistry analysis showed that both the types of OSs were positive of osteogenic (osteocalcin and osteonectin) and mesenchymal (vimentin) markers, whereas chondrogenic markers (COLL2 and S100) were negative in 3H-JUN cells and only

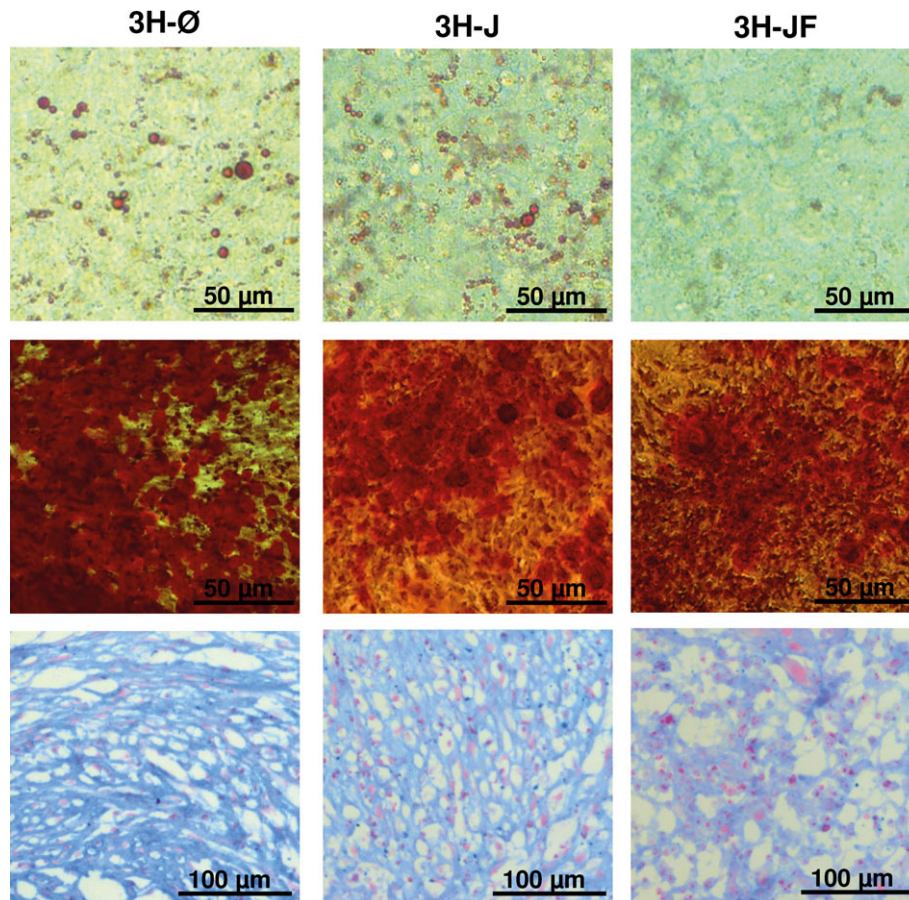


Figure 3. c-JUN or c-JUN/c-FOS overexpression in immortalized human mesenchymal stem cell does not affect their *in vitro* osteochondrogenic potential. Representative images of oil red O (up), alizarin red (middle), and alcian blue (bottom) staining after *in vitro* adipogenic, osteogenic, and chondrogenic differentiation of 3H (3H-Ø), 3H-JUN (3H-J), and 3H-JUN/FOS (3H-JF) cells ($n = 6$). Scale bars = 50 and 100 μm

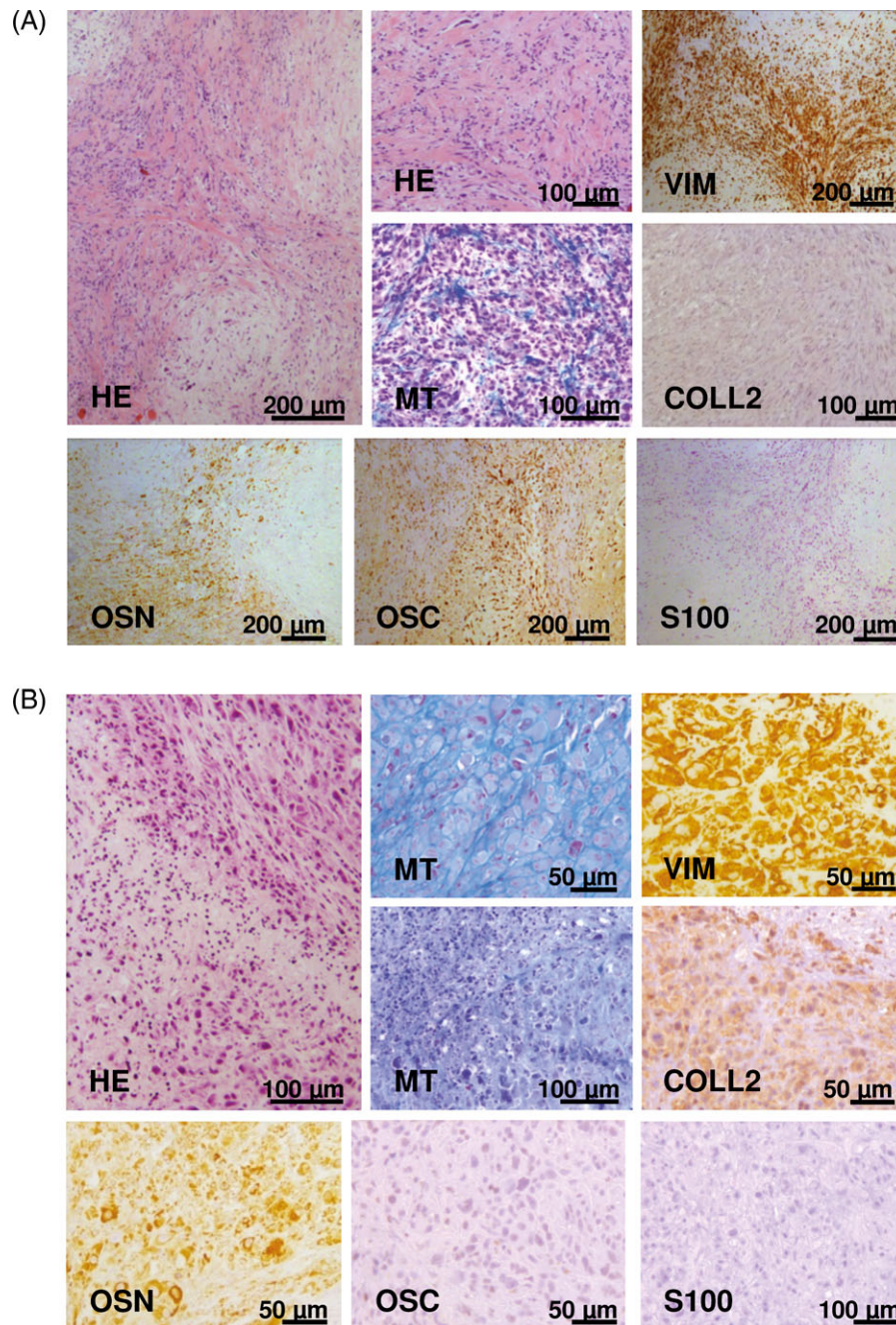


Figure 4. Ectopic inoculation of 3H-JUN and 3H-JUN/FOS cells generates osteosarcomas with fibroblastic and pleomorphic phenotypes. Representative images of the histological analysis of tumors generated after the subcutaneous inoculation of 3H-JUN (A) or 3H-JUN/FOS cells (B). (A) Hematoxylin/eosin and Masson's trichrome staining evidence that 3H-JUN cells form osteosarcoma (OS) characterized for osteoid deposition promoted by fibroblastic cells positive for osteogenic differentiation (osteocalcin [OSC] and osteonectin [OSN]) and mesenchymal (human vimentin) markers. In addition, tumor cells are negative for chondrogenic markers (COLL2 and S100). (B): 3H-JUN/FOS cells generate pleomorphic OS characterized by the expression of OSN and to a lesser extension of OSC. These tumors also display dispersed areas showing a myxoid chondrogenic phenotype and positivity for collagen type II marker. Scale bars = 50, 100, and 200 μm. Abbreviations: COLL2, collagen type II; HE, hematoxylin/eosin; MT, Masson's trichrome; OSC, osteocalcin; OSN, osteonectin; S100, S100 calcium binding protein; VIM, human vimentin.

partially positive (dispersed areas of COLL2 staining) in 3H-JUN/FOS cells (Fig. 4 and Table 1).

To further characterize the ability of cells overexpressing c-JUN or c-JUN/c-FOS to initiate OS formation in ectopic conditions which better mirror bone environmental conditions, we use a previously described ceramic model in which cells were

embedded in hydroxyapatite (HA)/tricalcium phosphate, as calcified substrates that resemble bone calcified extracellular matrix, in the presence or absence of an osteoinductive factor abundant in the bone milieu such as BMP2 [7, 26]. Subcutaneous implantation of these models resulted in the formation of OS with similar phenotypes than those observed after direct

inoculation of cells. Thus, 3H-JUN cells generated osteoid-forming tumors organized in longitudinal fibers with fibroblastic phenotype (Supporting Information Fig. S2) and, on the other hand, 3H-JUN/FOS tumors are formed by osteoid-forming pleomorphic cells and include areas of myxoid phenotype in response to HA and BMP2 stimulation (Supporting Information Fig. S2).

In summary, our results show that the overexpression of c-JUN or C-JUN and c-FOS fully transforms immortalized hMSCs giving rise to OS presenting different phenotypes *in vivo*.

Orthotopic *in vivo* Inoculation of 3H-JUN and 3H-JUN/FOS Cells Generate Phenotypically Different OSs

Bone environment has been proved to play essential roles in OS development [7, 27]. Therefore, we studied whether the inoculation of the cells in an orthotopic model could modulate the tumor phenotype observed after ectopic inoculation. Both 3H-JUN and 3H-JUN/FOS cells generated tumors when inoculated in the proximal tibia of immunodeficient mice. 3H-JUN cells presented a higher latency and a lower incidence (Supporting Information Table S5) and developed tumors that moderately affected bone cortex as confirmed by micro-computed tomography analysis (Fig. 5). In contrast, 3H-JUN/FOS cells showed a more aggressive phenotype; the mice that rapidly developed osteolytic lesions are able to compromise the limb structure and functionality (Fig. 5). Histological study indicated that both the cell lines formed OS. Tumors formed by 3H-JUN cells were composed of spindle-shaped cells which produced a small amount of osteoid matrix. These tumoral cells were organized in a fibroblastic geometry and displayed a herringbone pattern (Fig. 6A). On the other hand, 3H-JUN/FOS cells developed tumors presenting large osteogenic areas and aberrant trabeculae formation promoted by pleomorphic cells (Fig. 6B). Immunohistochemistry analysis also confirmed OS diagnosis (Fig. 6; Table 1). In both the cases, tumors presented

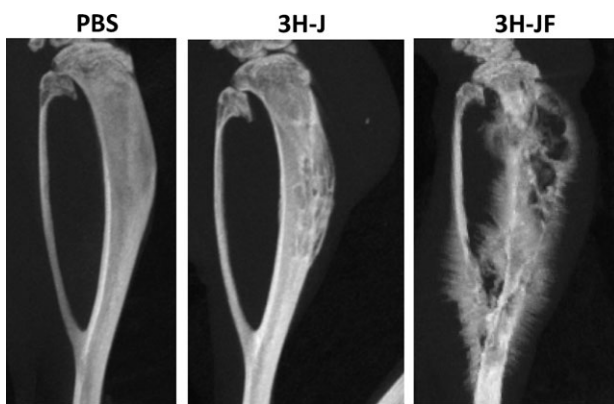


Figure 5. Micro-computed tomography imaging of osteosarcomas formed upon intrabone inoculation of 3H-JUN and 3H-JUN/FOS cells. Representative radiographic images (sagittal plane) showing mice tibiae inoculated with vehicle (phosphate-buffered saline; left panel), 3H-JUN (3H-J; middle panel), or 3H-JUN/FOS (3H-JF; right panel) cells. Mice inoculated with 3H-JUN develop tumors presenting moth-eaten geographic lesions affecting bone cortex, while those inoculated with 3H-JUN/FOS cells develop more aggressive tumors presenting a highly osteolytic phenotype which is also characterized by a prominent speculated periosteal reaction with sunburst appearance. Abbreviation: PBS, phosphate-buffered saline.

immunoreactivity for typical osteogenic (osteocalcin, osteonectin) and mesenchymal (vimentin) markers, while staining for chondrogenic markers (S100 and collagen II) was focal and limited to small areas.

Altogether, these results show that the overexpression of c-JUN or c-JUN and c-FOS is relevant to transforming events that are able to initiate osteosarcomagenesis from hMSCs independent of microenvironment factors. c-JUN overexpression is linked to the appearance of a fibroblastic phenotype, whereas the double overexpression of c-JUN and c-FOS shifts the phenotype to that observed in pleomorphic osteoblastic OS.

c-JUN and c-JUN/c-FOS Overexpression Induces *in vitro* Changes in NF- κ B Activity and Cytokines Secretion

Our gene expression study uncovered significant changes in the mRNA levels of different cell-to-cell signaling molecules after cell transformation (GO molecular functions, Supporting Information Table S2). To further investigate the changes induced by c-JUN and C-JUN/c-FOS expression that could affect the local tumor microenvironment, we study the cytokine secretion profile of 3H-JUN and 3H-JUN/FOS cells *in vitro* (Supporting Information Fig. S3). The expression of c-JUN and c-JUN/c-FOS modulated the secretion of a panel of cytokines (Supporting Information Fig. S3A), which changes were in accordance with those observed in mRNA levels (Supporting Information Fig. S3B). Interestingly, 3H-JUN/FOS cells showed the more evident changes and most of the cytokines modulated in these cells were downregulated. Among the cytokines upregulated by c-JUN or C-JUN/c-FOS, PDGF-A transcription, and secretion was upregulated in both 3H-JUN and 3H-JUN/FOS cells, while DPPIV (or CD26) was specifically upregulated at both mRNA and protein levels in 3H-JUN/FOS cells (Fig. 7A, 7B). Our previous *in vivo* experiments show that 3H-JUN/FOS cells induced a more aggressive disease and osteoblastic tumor phenotype, while 3H-JUN cells induced a less aggressive fibroblastic OS. To test the relation between those specific cytokines and tumor phenotype, we studied their gene expression levels in a microarray dataset of OS clinical samples (pretreatment biopsies). As in 3H-JUN/FOS cells, high levels of DPPIV correlate to a worse prognosis and show a tendency to associate with an osteoblastic phenotype in human clinical samples (Fig. 7C). In addition, PDGF-A expression levels also correlated with prognosis, although they were not significantly different between patients presenting fibroblastic and osteoblastic phenotypes (Fig. 7D).

NF- κ B is a transcription factor complex frequently dysregulated in several cancer types; NF- κ B modulates the transcription of different genes involved in stress response and inflammation, including cytokines regulation. Therefore, we decided to test the activation status of this transcription factor following c-JUN and c-JUN/c-FOS overexpression in immortalized cells. To quantify NF- κ B activity, we transduced transformed hMSCs with a lentiviral vector expressing firefly luciferase reporter gene downstream of NF- κ B responsive transcriptional elements. Quantification of luciferase activity in efficiently transfected cells showed that 3H-JUN cells presented higher NF- κ B transcriptional activity than 3H- \emptyset and 3H-JUN/FOS cells (Fig. 7E). Therefore, a higher NF- κ B activation status in transformed cells *in vitro* correlated with a less

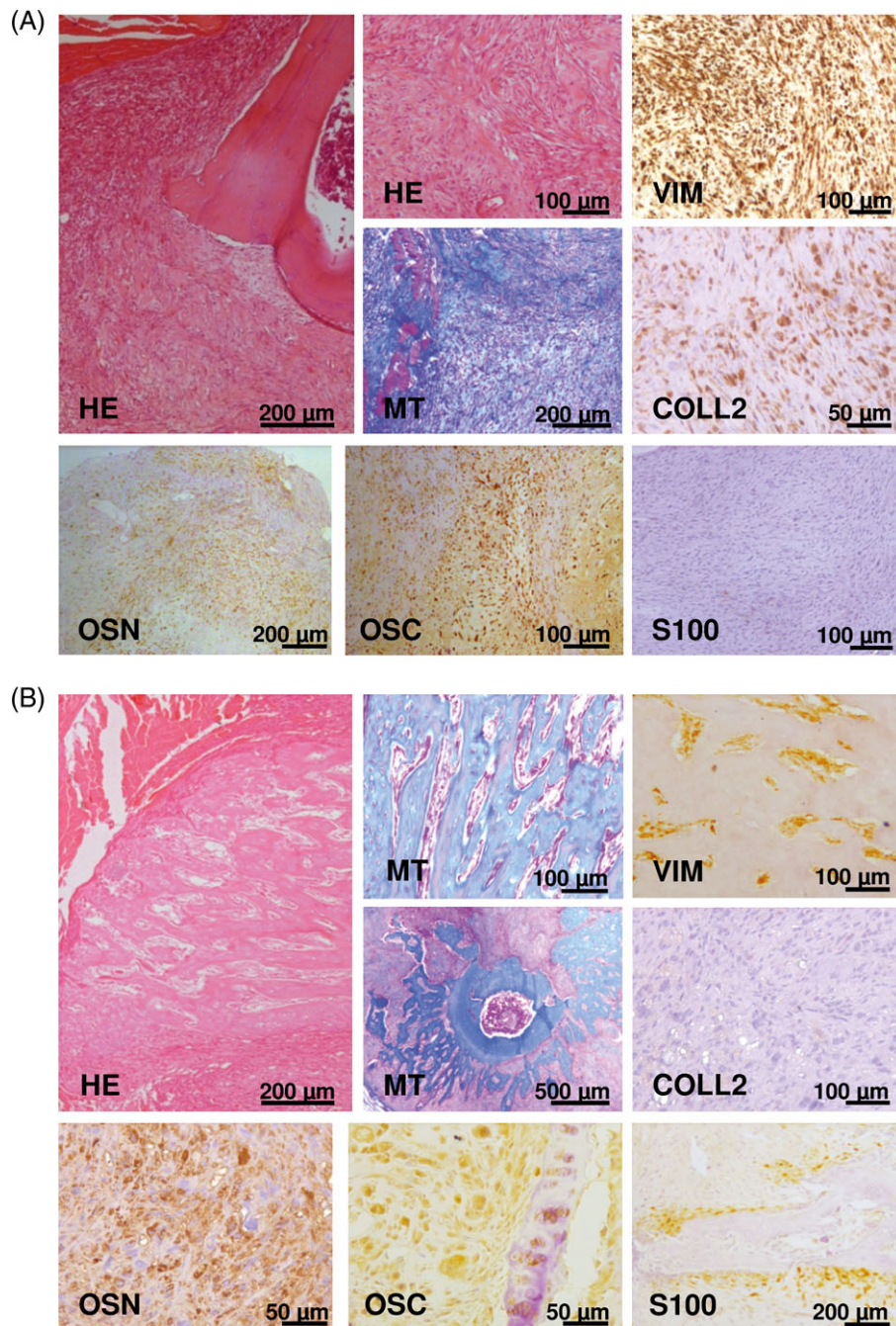


Figure 6. Orthotopic inoculation of 3H-JUN and 3H-JUN/FOS cells generates fibroblastic and pleomorphic osteoblastic osteosarcoma, respectively. Representative images of the histological analysis of tumors generated after the orthotopic inoculation of 3H-JUN (A) and 3H-JUN/FOS (B) cells. Hematoxylin/eosin and Masson's trichrome staining evidence the formation of osteosarcoma displaying osteoid matrix deposition generated by cells with fibroblastic morphology positive for osteogenic (osteocalcin and osteonectin) and mesenchymal (human vimentin) markers and partially positive (COLL2) or negative (S100) for chondrogenic markers. Scale bars = 50, 100, and 200 μm. Abbreviations: COLL2, collagen type II; HE, hematoxylin/eosin; MT, Masson's trichrome; OSN, osteonectin; OSC, osteocalcin; S100, S100 calcium binding protein; VIM, human vimentin.

aggressive disease and a fibroblastic phenotype of tumors. We further tested this association comparing the transcription levels of c-JUN, c-FOS, and different members of NF-κB transcription factor complexes in clinical samples. As in our model, the differential composition of AP-1 transcription factor determinate tumor phenotype, so in clinical samples, c-JUN expression levels do not associate with tumor phenotype, while c-FOS levels are upregulated in osteoblastic OS

tumors (Fig. 7F). Furthermore, similar to our model, in human samples transcription levels of the NF-κB components RELB, NFKB1, and NFKB2 correlate to a better overall survival and a fibroblastic OS phenotype (Fig. 7G–7I). In sum, our data point out the relevance of different AP-1 members in regulating NF-κB functionality, where low levels of NF-κB activity do associate to reduced patients survival and a specific tumor phenotype.

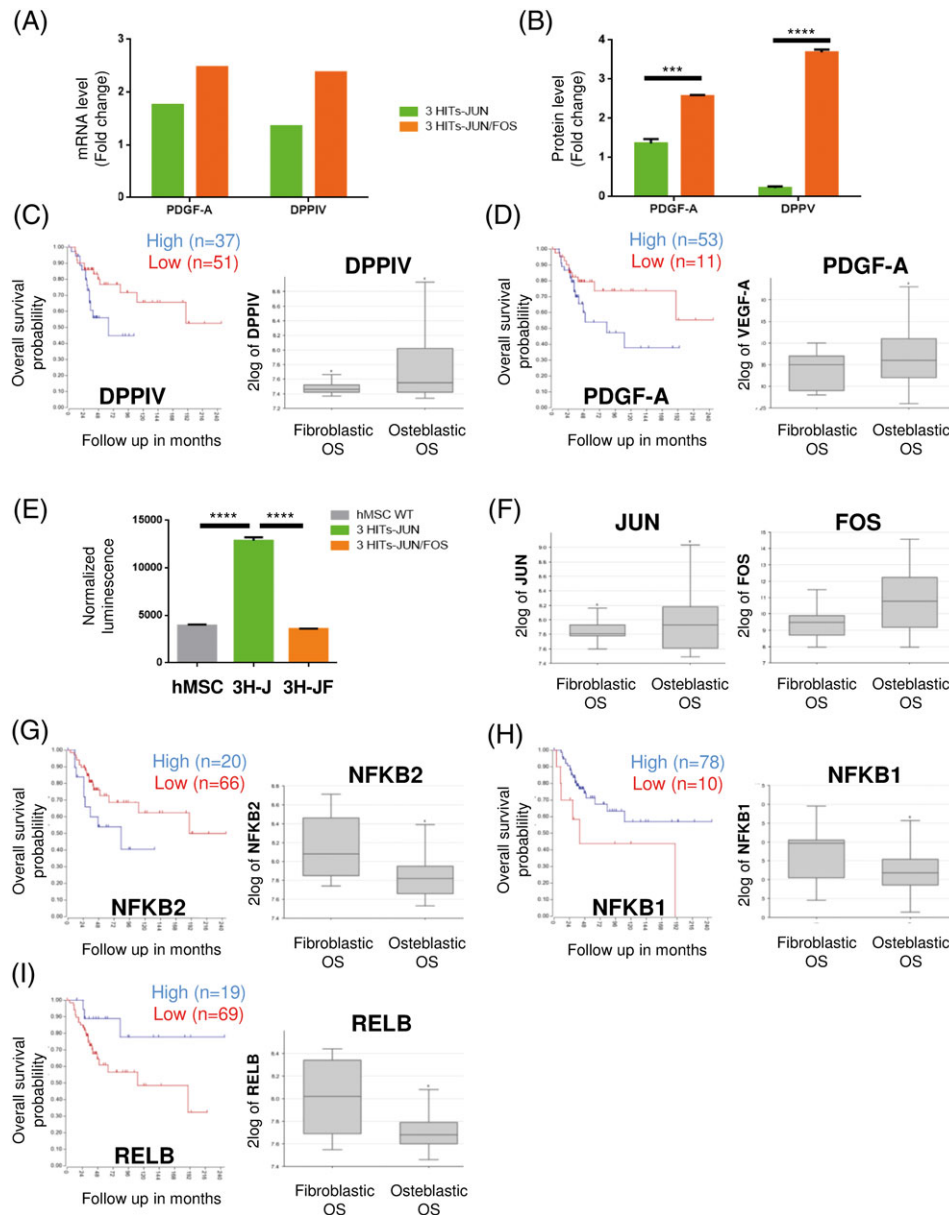


Figure 7. c-JUN or c-JUN/c-FOS overexpression in immortalized human mesenchymal stem cell induces changes in cytokines release and nuclear factor-kB pathway. (A) Dipeptidyl peptidase IV (DPPIV) and platelet-derived growth factor (PDGF)-A genes expression levels of transduced cells according to the values obtained in the microarray analysis presented in Figure 2. Data are presented as fold changes to control 3H-Ø cells. (B): Levels of DPPIV and PDGF-A secreted to the medium in 3H-JUN and 3H-JUN/FOS cultures. Data are presented as fold changes to control 3H-Ø cells. Error bars represent SEM. Statistic tests: two-way analysis of variance (ANOVA) and Bonferroni post hoc test, CI: 95%, alpha: 0.05. $p < .0001$ (****). (C) Kaplan–Meier survival analysis (left) and mRNA expression level (right) of DPPIV gene in human clinical samples. (D): Kaplan–Meier survival analysis (left) and mRNA expression level (right) of PDGF-A gene in human clinical samples. (E): NF-kB promoter activity in transduced cells. Data are normalized to lentiviral transduction efficiency. Statistic tests: two-way ANOVA and Bonferroni post hoc test, CI: 95%, alpha: 0.05. $p < .0001$ (****). (F): mRNA expression level of c-JUN and c-FOS genes in human clinical samples. (G, I): Kaplan -Meier survival analysis (left) and mRNA expression level (right) of NFKB2 (G), NFKB1 (H), and RELB (I) genes in human clinical sample dataset. mRNA expression levels are graphed as box plot where error bars represents maximum and minimum values. Statistic tests for Kaplan–Meier survival analysis and mRNA expression levels comparison are presented in Supporting Information Table S5. Abbreviations: DPPIV, dipeptidyl peptidase IV; OS, osteosarcoma; PDGF-A, platelet-derived growth factor-A.

DISCUSSION

Different studies support the idea that increased expression of AP-1 is associated with human tumorigenesis [28]. The overexpression of c-JUN or the combination of c-JUN/c-FOS in healthy hMSC is not sufficient to induce cell transformation; therefore, we studied the effect of their overexpression in

immortalized hMSCs. Confirming the oncogenic potential of the AP-1 complex, the expression of its components was sufficient to induce proliferation, alter cell cycle, induce morphological changes, and generate OS in vivo from immortalized hMSCs. Various studies have demonstrated that the differential dimerization between JUN and FOS members alters the promoter-binding activity, the transcriptional capacity, the

protein stability, and the transcriptional repertoire of the AP-1 complex [16, 29–31]. However, the differential role of homodimeric versus heterodimeric AP-1 complex in hMSCs biology is mostly unknown. To gain new insight, we studied the gene expression profile and the differential gene expression of immortalized hMSCs overexpressing c-JUN or c-JUN/c-FOS. According to the ability of the joined expression of c-JUN and c-FOS to dysregulate a higher number of genes, 3H-JUN/FOS cells showed more differentially expressed genes and higher enriched GO terms. More relevant alterations detected in gene expression studies were related to changes in cell cycle, proliferation, and differentiation processes, as genes with growth factor, cytokine, and chemokine activity. Indeed, transgenes expression in immortalized cells induced an increased secretion of PDGF-A. It was shown that PDGF-A overexpression generates an autocrine loop promoting OS cells growth and its expression was reported as prognostic factor and therapeutic target (Gleevec) in OSs [32] and soft tissue sarcomas [33]. Furthermore, PDGF-A exerts a paracrine effect as chemotactic and differentiating factor for mesenchymal cells [34] including MSCs. In this regard, different studies have investigated the role of healthy MSCs in tumor microenvironment, with opposite results of pro- and anti-tumorigenic effect on tumor growth and metastatic spread [35, 36]. Given their biological properties and their influence on tumor growth, MSCs represent cells with unique characteristic in both cell transformation and tumor microenvironment regulation [37].

Another interesting finding in our data is the augmented secretion of DPPIV of 3H-JUN/FOS cells, where its overexpression correlated with tumor aggressiveness and osteoblastic tumor phenotype in our samples. This finding was further confirmed in clinical data, where higher gene expression levels correlate to osteoblastic OS and a worse overall survival in patients. This signaling molecule was implicated in the immunological regulation and processing of different growth factors, cytokines, and chemokines. DPPIV/CD26 plays a specific role in osteoclast development [38], is associated with osteolytic lesions [39], and further represent a prognostic marker in OS [40]. Interestingly, this gene contains in its promoter putative binding sequences for both AP1 and NF- κ B transcription factors [41].

NF- κ B transcription factor has a well-known implication in oncogenesis; different reports showed that NF- κ B can function both as an oncogene or tumor suppressor gene depending on the cell context and cancer type [42]. NF- κ B activation was associated with osteosarcomagenesis [43, 44], where the inhibition of this factor in cell lines was sufficient to revert malignant development [45]. In our study, we found that the homodimeric or heterodimeric composition of AP1 can differentially modulate NF- κ B activity, correlating also to specific tumor phenotype and tumor aggressiveness. Thus, in accordance with the ability of 3H-JUN cells to induce fibroblastic OS with a less aggressive disease development and high levels of NF- κ B activity, a higher expression of different members of NF- κ B complex correlates to an increased overall survival and/or to fibroblastic OS phenotype in clinical samples. Similarly, the fact that 3H-JUN/FOS cells induce osteoblastic OS showing a more aggressive disease and lower levels of NF- κ B activity, parallels the finding in clinical samples where a lower expression of NF- κ B complex members correlates to OS with an osteoblastic phenotype and a more aggressive behavior.

Previous studies of our laboratory indicated that c-FOS overexpression in immortalized hMSC generated chondrogenic tumors. The data presented here complete this frame suggesting that the overexpression of AP-1 factor in hMSCs is a key factor in the development of different bone tumors and that abundance of the different homo/heterodimers of this transcription factor could modulate the final phenotype. c-JUN overexpression would be specifically associated with the development of OS and that the concurrent enhanced expression of c-FOS could modulate the aggressiveness and the phenotype of the OS. Importantly, OS tumor phenotype was recognized as prognostic factor. In this line, osteoblastic OS patients displayed up to 20% lower 5-year event-free survival rates than patients with the fibroblastic phenotype [46, 47]. Resembling this clinical observation, our model of c-JUN-expressing fibroblastic OS showed a less aggressive behavior than the c-JUN/c-FOS expressing pleomorphic conventional OS. Thus, signs of malignancy, such as the presence of cortical breakthrough, soft tissue mass generation, permeative development, and periosteal reaction were much more evident in tumors developed by c-JUN/c-FOS overexpressing cells. On the other hand, the geographic and moth-eaten pattern of bone destruction observed in tumors derived from 3H-JUN cells represented less malignant lesions. Higher tumor incidence and lower latency were observed with 3H-JUN/FOS cells compared with 3H-JUN cells. Altogether, these data support the idea that some genetic hits could be effectively responsible for inducing MSCs transformation and at the same time, a specific tumor phenotype. Furthermore, the effect of this alteration is not restricted only to the inner cell differentiation program but is extended, with a pattern of signaling molecules, to the tumor microenvironment. Specifically, our two models of OS based on the overexpression of c-JUN or c-JUN and c-FOS reflect different phenotypes and behaviors of the human disease.

In the clinical setting, AP-1 may represent a promising drug target due to its implication in tumor development and progression. Different studies have provided evidence that drugs like glucocorticoids, dexamethasone, heparin, and aspirin or other more natural compounds, like green tea polyphenols, oil fish, curcumin, and cannabidiol could modulate AP-1 functions [48, 49]. These and other AP-1 inhibitors could effectively interfere with oncogene-induced transformation and tumor cell growth, although their effectiveness in OS treatment still requires a thorough investigation. Our results highlight the relevant role that AP-1 factors may play in OS development, and suggest their possible use as biomarkers for patient stratification and future therapeutic design.

CONCLUSION

Our findings uncover the implication of AP-1 complex in osteosarcomagenesis. Our study shows that some genetic hits could be responsible for inducing MSCs transformation and simultaneously, a specific tumor phenotype. Here, we found that the overexpression of different AP-1 complex members can give rise to OS presenting specific phenotypes. Specifically, overexpression of c-JUN induces fibroblastic OS and c-JUN/c-FOS osteoblastic OS, where NF- κ B transcription factor would have a role in determining these different tumor entities.

ACKNOWLEDGMENTS

We thank Fernando González for assistance in confocal microscopy studies, Jesús García-Cantalejo for assistance in microarray studies, and Javier Alonso for assistance in GSEA studies. This work was supported by grants from the Fondo de Investigaciones Sanitarias (FIS: PI11/00377 [to J.G.-C.]; and RTICC: RD12/0036/0027 [to J.G.-C.], RD12/0036/0020 [to S.N.]; Consorcio CIBERONC CB16/12/00390 [to R.R.] and CB16/12/00484 [to S.N.]; Miguel Servet II Program CPII16/00049 [to R.R.]; and Sara Borrell CD16/13/00103 [to S.T.M.] and CD11/00132 [to A.A.]); The Juan de la Cierva program JCI-2010-06123 [to A.A.]; the Agencia Estatal de Investigación (AEI) (MINECO/Fondo Europeo de Desarrollo Regional [FEDER]: SAF-2016-75286-R [to R.R.]); and the Madrid Regional Government (CellCAM; P2010/BMD-2420 [to J.G.-C.]) in Spain.

AUTHOR CONTRIBUTIONS

S.G. and A.A.: development of methodology, conception and design, acquisition, analysis, interpretation of data and manuscript writing; M.A.R.-M., F.M., S.T.M., R.R. and S.N.: acquisition, analysis, and interpretation of data; J.G.-C.: Conception, design, analysis and interpretation of data, financial support, manuscript writing and Senior authorship. S.G., and A. A. contributed equally to this article. The manuscript has been seen and approved by all authors.

DISCLOSURE OF POTENTIAL CONFLICTS OF INTEREST

The authors indicated no potential conflicts of interest.

REFERENCES

- ESMO/European Sarcoma Network Working Group. Bone sarcomas: ESMO Clinical Practice Guidelines for diagnosis, treatment and follow-up. *Ann Oncol* 2014;25:113–123.
- Broadhead ML, Clark JC, Myers DE, et al. The molecular pathogenesis of osteosarcoma: a review. *Sarcoma*. 2011;2011:959248.
- Martin JW, Squire JA, Zielenska M. The genetics of osteosarcoma. *Sarcoma* 2012;2012:e627254.
- Gorlick R. Current concepts on the molecular biology of osteosarcoma. *Cancer Treat Res* 2009;152:467–478.
- Ng AJ, Mutsaers AJ, Baker EK et al. Genetically engineered mouse models and human osteosarcoma. *Clin Sarcoma Res* 2012;2:19.
- Rubio R, Gutierrez-Aranda I, Sáez-Castillo AI et al. The differentiation stage of p53-Rb-deficient bone marrow mesenchymal stem cells imposes the phenotype of in vivo sarcoma development. *Oncogene* 2013;32:4970–4980.
- Rubio R, Abarrategi A, Garcia-Castro J et al. Bone environment is essential for osteosarcoma development from transformed mesenchymal stem cells. *STEM CELLS* 2014;32:1136–1148.
- Rodríguez R, Rubio R, Menendez P. Modeling sarcomagenesis using multipotent mesenchymal stem cells. *Cell Res* 2012;22:62–77.
- Funes JM, Quintero M, Henderson S et al. Transformation of human mesenchymal stem cells increases their dependency on oxidative phosphorylation for energy production. *Proc Natl Acad Sci USA* 2007;104:6223–6228.
- Li N, Yang R, Zhang W et al. Genetically transforming human mesenchymal stem cells to sarcomas: Changes in cellular phenotype and multilineage differentiation potential. *Cancer* 2009;115:4795–4806.
- Serakinci N, Guldborg P, Burns JS et al. Adult human mesenchymal stem cell as a target for neoplastic transformation. *Oncogene* 2004;23:5095–5098.
- Yang Y, Yang R, Roth M et al. Genetically transforming human osteoblasts to sarcoma: Development of an osteosarcoma model. *Genes Cancer* 2017;8:484–494.
- Wang J-Y, Wu P-K, PC-H C et al. Generation of osteosarcomas from a combination of Rb Silencing and c-Myc overexpression in human mesenchymal stem cells. *STEM CELLS TRANSLATIONAL MEDICINE* 2017;6:512–526.
- Rodríguez R, Rubio R, Gutierrez-Aranda I et al. FUS-CHOP fusion protein expression coupled to p53 deficiency induces liposarcoma in mouse but not in human adipose-derived mesenchymal stem/stromal cells. *STEM CELLS* 2011;29:179–192.
- Rodríguez R, Tornin J, Suarez C et al. Expression of FUS-CHOP fusion protein in immortalized/transformed human mesenchymal stem cells drives mixoid liposarcoma formation. *STEM CELLS* 2013;31:2061–2072.
- Zhou H, Zarubin T, Ji Z et al. Frequency and distribution of AP-1 sites in the human genome. *DNA Res* 2005;12:139–150.
- Wagner EF. Functions of AP1 (Fos/Jun) in bone development. *Ann Rheum Dis* 2002;61:40–42.
- Jochum W1, Passequé E, Wagner EF. AP-1 in mouse development and tumorigenesis. *Oncogene* 2001;20:2401–2412.
- Franchi A, Calzolari A, Zampi G. Immunohistochemical detection of c-fos and c-jun expression in osseous and cartilaginous tumours of the skeleton. *Virchows Arch* 1998;432:515–519.
- Stein B, Baldwin AS, Ballard DW et al. Cross-coupling of the NF-kappa B p65 and Fos/Jun transcription factors produces potentiated biological function. *EMBO J* 1993;12:3879–3891.
- Wang X, Sonenshein GE. Induction of the RelB NF-kB subunit by the cytomegalovirus IE1 protein is mediated via Jun kinase and c-Jun/Fra-2 AP-1 complexes. *J Virol* 2005;79:95–105.
- Wei W, Sedivy JM. Differentiation between senescence (M1) and crisis (M2) in human fibroblast cultures. *Exp Cell Res* 1999;253:519–522.
- Wilson AA, Kwok LW, Porter EL et al. Lentiviral delivery of RNAi for in vivo lineage-specific modulation of gene expression in mouse lung macrophages. *Mol Ther* 2013;21:825–833.
- Ritchie ME, Phipson B, Wu D et al. limma powers differential expression analyses for RNA-sequencing and microarray studies. *Nucl Acids Res* 2015;43:e47.
- Kuijjer ML, Rydbeck H, Kresse SH et al. Identification of osteosarcoma driver genes by integrative analysis of copy number and gene expression data. *Genes Chromosomes Cancer* 2012;51:696–706.
- Abarrategi A, Perez-Tavarez R, Rodríguez-Milla MA et al. In vivo ectopic implantation model to assess human mesenchymal progenitor cell potential. *Stem Cell Rev* 2013;9:833–846.
- Alfranca A, Martinez-Cruzado L, Tornin J et al. Bone microenvironment signals in osteosarcoma development. *Cell Mol Life Sci* 2015;72:3097–3113.
- Eferl R, Wagner EF. AP-1: A double-edged sword in tumorigenesis. *Nat Rev Cancer* 2003;3:859–868.
- Wang W-M, Wu S-Y, Lee A-Y et al. Binding site specificity and factor redundancy in activator protein-1-driven human papillomavirus chromatin-dependent transcription. *J Biol Chem* 2011;286:40974–40986.
- Chinenov Y, Kerppola TK. Close encounters of many kinds: Fos-Jun interactions that mediate transcription regulatory specificity. *Oncogene* 2001;20:2438–2452.
- Li M, Ge Q, Wang W et al. c-Jun binding site identification in K562 cells. *J Genet Genomics* 2011;38:235–242.
- Kubo T, Piperdi S, Rosenblum J et al. Platelet-derived growth factor receptor as a prognostic marker and a therapeutic target for imatinib mesylate therapy in osteosarcoma. *Cancer* 2008;112:2119–2129.
- Pender A, Jones RL. Olaratumab: a platelet-derived growth factor receptor- α -blocking antibody for the treatment of soft tissue sarcoma. *Clin Pharmacol* 2017;9:159–164.
- Sulzbacher I, Träxler M, Mosberger I et al. Platelet-derived growth factor-AA and -alpha receptor expression suggests an autocrine and/or paracrine loop in osteosarcoma. *Mod Pathol* 2000;13:632–637.
- Paino F, La Noce M, Di Nucci D et al. Human adipose stem cell differentiation is highly affected by cancer cells both in vitro and in vivo: implication for autologous fat grafting. *Cell Death Dis* 2017;8:e2568.
- Zheng Y, Wang G, Chen R et al. Mesenchymal stem cells in the osteosarcoma

microenvironment: Their biological properties, influence on tumor growth, and therapeutic implications. *Stem Cell Res Ther* 2018;9:22.

37 Papaccio F, Paino F, Regad T et al. Concise review: Cancer cells, cancer stem cells, and mesenchymal stem cells: Influence in cancer development. *STEM CELLS TRANSLATIONAL MEDICINE* 2017;6:2115–2125.

38 Hiroko N, Hiroshi S, Hiroko M et al. Blockade of CD26 signaling inhibits human osteoclast development. *J Bone Mineral Res* 2014;29:2439–2455.

39 Nishida H, Madokoro H, Suzuki H et al. CD26 is a novel target for the treatment of tumor progression and its related osteolytic bone disease in multiple myeloma. *Blood* 2015;126:1809–1809.

40 Zhang H, Lin H, Mo X et al. Synergistic relationship between dipeptidyl peptidase IV and neutral endopeptidase expression and

the combined prognostic significance in osteosarcoma patients. *Med Oncol* 2013;30:608.

41 Bauvois B, Djavaheri-Mergny M, Rouillard D et al. Regulation of CD26/DPPIV gene expression by interferons and retinoic acid in tumor B cells. *Oncogene* 2000;19:265–272.

42 Xiao X, Yang G, Bai P et al. Inhibition of nuclear factor-kappa B enhances the tumor growth of ovarian cancer cell line derived from a low-grade papillary serous carcinoma in p53-independent pathway. *BMC Cancer* 2016;16:582.

43 Tang Q-L, Xie X-B, Wang J et al. Glycogen synthase kinase-3 β , NF- κ B signaling, and tumorigenesis of human osteosarcoma. *J Natl Cancer Inst* 2012;104:749–763.

44 Lu J, Song G, Tang Q et al. IRX1 hypomethylation promotes osteosarcoma metastasis via induction of CXCL14/NF- κ B signaling. *J Clin Invest* 2015;125:1839–1856.

45 Andela VB, Sheu TJ, Puzas EJ et al. Malignant reversion of a human osteosarcoma cell line, Saos-2, by inhibition of NF κ B. *Biochem Biophys Res Commun* 2002;297:237–241.

46 Bacci G, Longhi A, Versari M et al. Prognostic factors for osteosarcoma of the extremity treated with neoadjuvant chemotherapy. *Cancer* 2006;106:1154–1161.

47 Ferrari S, Bertoni F, Mercuri M et al. Predictive factors of disease-free survival for non-metastatic osteosarcoma of the extremity: An analysis of 300 patients treated at the Rizzoli Institute. *Ann Oncol* 2001;12:1145–1150.

48 Keri G, Toth I. *Molecular Pathomechanisms and New Trends in Drug Research*. CRC Press, Boca Raton, FL, 2003.

49 Ye N, Ding Y, Wild C et al. Small molecule inhibitors targeting activator protein 1 (AP-1). *J Med Chem* 2014;57:6930–6948.



See www.StemCells.com for supporting information available online.